# Synthesis of N$_2$-Type Superatomic Molecules

Ryohei Saito,[†‡] Katsuhiro Isozaki,[†‡*] Yoshiyuki Mizuhata,[†] and Masaharu Nakamura[†‡*]

†Institute for Chemical Research, Kyoto University, Uji, Kyoto 611-0011, Japan

‡Department of Energy and Hydrocarbon Chemistry, Graduate School of Engineering, Kyoto University, Nishikyo-ku, Kyoto 615-8510, Japan

ABSTRACT: Exploration of multiple bonds between superatoms remains uncharted territory. In this study, we present the synthesis and characterization of N$_2$-type superatomic molecules featuring triple bonds between two superatoms. The successful synthesis of M$_2$Au$_{17}$ (M = Pd, Pt) nanoclusters hinged upon the photo-induced fusion of MAu$_{12}$ superatoms, achieved through sequential electron transfer and detachment of [AuPR$_3$]$^+$ species. Solid-state structures were confirmed via X-ray crystallography, while their electronic structures were elucidated through density functional theory (DFT) calculations. Analysis of electronic absorption properties, coupled with time-dependent DFT calculations, unveiled a symmetry-dependent electron transition nature between superatomic molecular orbitals, akin to those observed in conventional molecules.
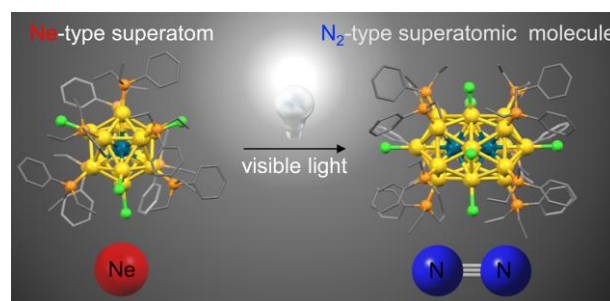
■ INTRODUCTION

Ligand-protected gold nanoclusters exhibit unique properties depending on the ligand type, number of atoms, and overall structure.[1–4] They have gained considerable attention as functional materials in catalysts, photosensitizers, luminescent materials, etc. In particular, a "cluster of clusters" with an Au$_{13}$ core as the building block often has an electronic structure similar to that of conventional molecules, owing to the formation of superatomic molecular orbitals (SAMOs) originating from the linear combination of superatomic orbitals (SAOs) under the supervalence bond model.[4–12] Such gold nanoclusters are called superatomic molecules and display attractive physical properties and reactivity. Two kinds of gold nanoclusters, Au$_{38}$(SR)$_{24}$[9,10] and [Au$_{20}$(PPhpy$_2$)$_{10}$Cl$_4$]Cl$_2$,[11,12] are recognized as F$_2$-type superatomic molecules bearing a single bond between the superatoms, because their 14 valence electrons in the (Au$_{23}$)$^{9+}$ and (Au$_{20}$)$^{6+}$ cores are accommodated in the SAMOs to form an electron configuration of $(1\Sigma_s)^2(1\Sigma^*_s)^2(1\Pi_{px,py})^4(1\Sigma_{pz})^2(1\Pi_{px,py}^*)^4$. Based on the formation of F$_2$-like SAMOs in Au$_{38}$(SR)$_{24}$, Pd- or Pt-doped M$_2$Au$_{36}$(SR)$_{24}$[13–18] were also expected to be O$_2$-type superatomic molecules due to their 12 valence electrons in the (M$_2$Au$_{21}$)$^{9+}$ core. However, a recent study by Tsukuda based on single-crystal X-ray diffraction (SCXRD) analysis and density functional theory (DFT) calculations revealed that the 1P SAOs of each M@Au$_{12}$ core were combined in the bent configuration, resulting in an electron configuration of $(1A_1)^2(1B_2)^2(2A_1)^2(3A_1)^2(1B_1)^2(2B_2)_2$ that does not resemble O$_2$.[14] The theoretical study by Yang et al. predicted a N$_2$-like electron configuration for the [Ag$_{32}$(dppe)$_5$(SC$_6$H$_4$CF$_3$)$_{24}$]$^{2-}$ cluster having 10 valence electrons.[19] However, the formula in the reported crystallographic data indicates that the cluster is a monoanion [Ag$_{32}$(dppe)$_5$(SC$_6$H$_4$CF$_3$)$_{24}$]$^-$ having 9 valence electrons instead.[20] Onaka et al. reported the synthesis and structural determination of Au$_{12}$Ag$_7$(PMe$_2$Ph)$_{10}$(NO$_3$)$_9$ nanocluster having 10 valence electrons but did not investigate its electronic structure.[21] Overall, there are no synthetic examples of O$_2$- and N$_2$-type superatomic molecules that are expected to have SAMOs corresponding to multiple bonds. Therefore, the bonding theory and photophysical nature of superatomic molecules remain unexplored.

To address this issue, synthetic methods for gold nanoclusters with such SAMOs have been developed in recent years by using nanoclusters with a reactive Au$_{13}$ or heterometal-doped MAu$_{12}$ (M = Pd, Pt) core as a precursor (Figure 1).[13,14] Maran and co-workers reported that Au$_{38}$(SR)$_{24}$ (14e) can be synthesized using [Au$_{25}$(SR)$_{18}$]^0 (7e)[22–24] having an open-shell electron configuration (Figure 1a).[25] Tsukuda and co-workers also achieved the synthesis of M$_2$Au$_{36}$(SR)$_{24}$ (12e) (M = Pd, Pt) by reacting hydride-activated [MAu$_8$(PPh$_3$)$_8$]$^{2+}$ (8e)[26,27] and monoanionic [MAu$_{24}$(SR)$_{18}$]$^-$ (7e)[28] (Figure 1b).[13,14] These facts suggest that nanoclusters with SAMO may be synthesized by using nanoclusters with highly reactive Au$_{13}$ or MAu$_{12}$ cores as precursors.

Here, we report a novel synthetic protocol for superatomic molecules triggered by photo-irradiation (Figure 1c), in which the photo-induced fusion reaction of M@Au$_{12}$ (M = Pd, Pt) superatoms occurs efficiently to afford unprecedented M$_2$Au$_{17}$ superatomic molecules. SCXRD and electrospray ionization-mass spectrometry (ESI-MS) analyses revealed that the M$_2$Au$_{17}$ core was composed of two MAu$_{12}$ structural units sharing an Au$_5$ facet and a neutral state bearing 10
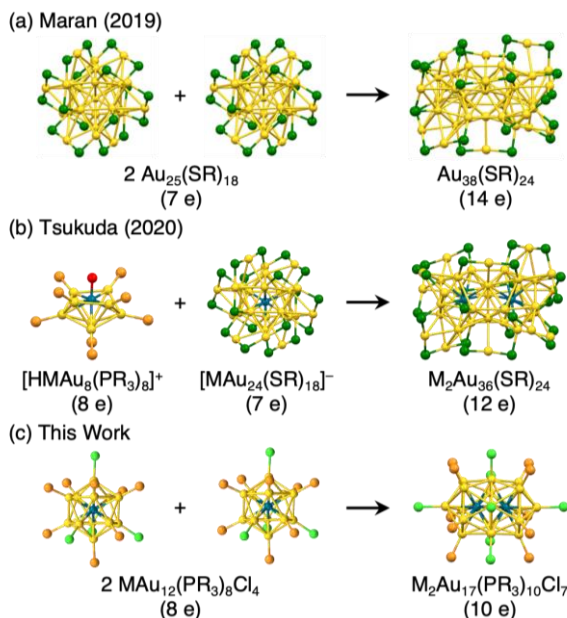
Figure 1. (a) Fusion of two 7e $Au_{25}(SR)_{18}$ clusters. (b) Fusion between hydride-activated 8e $[HMAu_8(PR_3)_8]^+$ cluster and 7e $[MAu_{24}(SR)_{18}]^-$ sluter. (c) Photo-induced fusion of two 8e $MAu_{12}(PR_3)_8Cl_4$ clusters.

valence electrons. DFT calculations clarified that the SAOs of two icosahedrons were combined to construct the SAMOs having the electron configuration of $(1\Sigma_s)^2(1\Sigma_s*)^2(1\Pi_{px, py})^4(1\Sigma_{pz})^2$, similar to that of N_2 molecule. Furthermore, electronic absorption measurements and time-dependent DFT (TDDFT) calculations proved the molecule-like electron excitation property of the superatomic molecules, based on the symmetry-allowed electron transition between SAMOs under the Laporte rule.[29] This is the first report of both experimentally and theoretically determined N_2-type superatomic molecules and their symmetry-dependent electron transition.

■ RESULTS AND DISCUSSION

The precursor $MAu_{12}(depp)_8Cl_4$ (**1a**: M = Pd, **1b**: M = Pt, depp = diethylphenylphosphine) nanoclusters were synthesized by a co-reduction method and fully characterized by ESI-MS, UV-Vis absorption spectroscopy, and SCXRD (Figures S1 and S2). Then, the $M_2Au_{17}(depp)_{10}Cl_7$ nanoclusters (**2a**: M = Pd, **2b**: M = Pt) were synthesized under photo irradiation (Scheme 1). When the MeOH/dichloromethane (DCM) solutions of **1** were irradiated, the absorption spectra gradually changed, and new absorption bands appeared at 730 nm for **1a** and 700 nm for **1b** (for the time courses of UV-Vis absorption spectra see Figures S3 and S4). Finally, crystalline nanoclusters were obtained by isolation using PTLC and recrystallization. An earlier study by Migos reported the synthesis of icosahedral Au_{13} nanocluster using dimethylphosphine (dmpe) ligand,[30] but dmpe resulted in producing a mixture of nanocluster products during $PdAu_{12}$ nanocluster due to the less steric bulkiness. The photo irradiation was also investigated using a Au_{13} nanocluster with a trialkylphosphine, reported by Wang,[31] but no reaction took place, indeed the progress of a similar fusion reaction with MAu_{12} derivatives. These results indicate the proper bulkiness of phosphine ligand and the doping of metal are the keys to this photoinduced fusion reaction.

Scheme 1. Photo-Induced Synthesis of $M_2Au_{17}(depp)_{10}Cl_7$

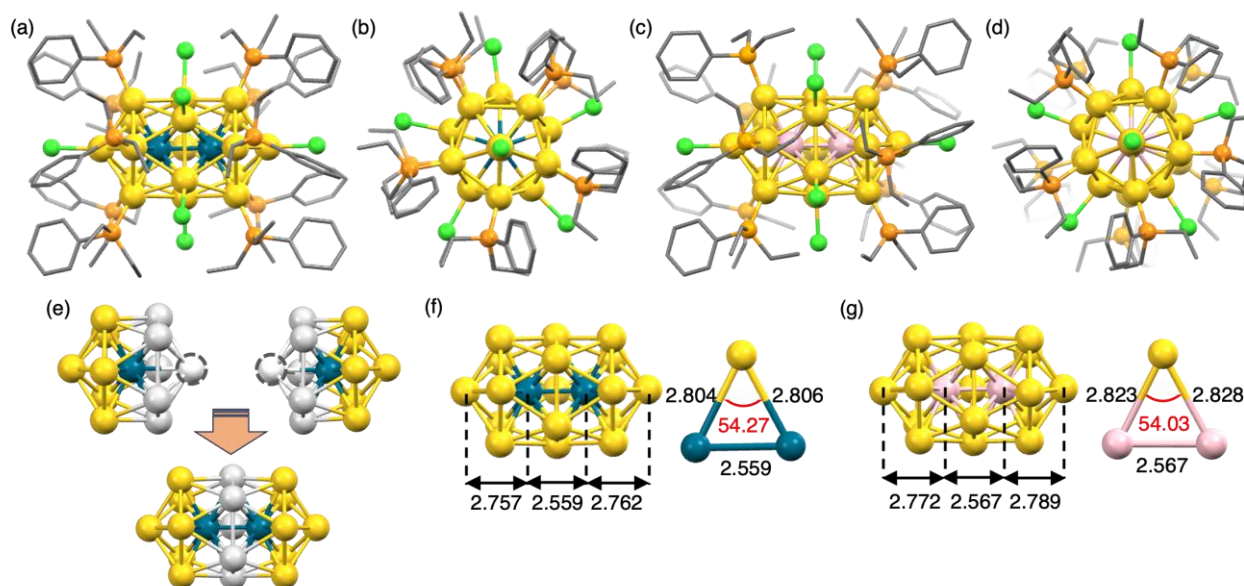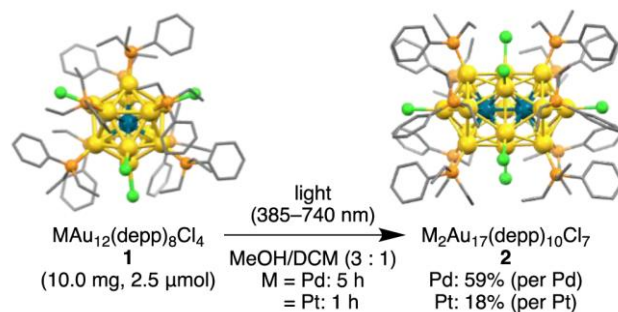**Figure 2.** Crystal structures of $Pd_2Au_{17}(depp)_{10}Cl_7$ **2a** in (a) front view and (b) side view and of $Pt_2Au_{17}(depp)_{10}Cl_7$ **2b** in (c) front view and (d) side view. Color code: dark-blue, Pd; pink, Pt; yellow, Au; orange, P; yellow-green, Cl. The H atoms are omitted for clarify. (e) Anatomy of Pd_2Au_{17} core in **2a**, white atoms denote the shared Au_5 facet and dot-circled atoms are replaced by another Pd atoms. (f), (g) Characteristic bond lengths and angles of Pd_2Au_{17} and Pt_2Au_{17} core.

SCXRD analyses unequivocally determined the molecular structures of **2** (Figures 2a–d). The M_2Au_{17} core is likely formed by the fusion of two MAu_{12} nanoclusters sharing six Au atoms, in which the Au_5 facet is shared and one Au atom is replaced by Pd or Pt (Figure 2e). Seven chloride atoms are bound to the two vertex sites and five shared Au atoms, while 10 depp ligands are coordinated to the remaining 10 surface Au atoms, resulting in a total structure with D_{5h} symmetry. Although the position of Pt atoms in **2b** cannot be determined by SCXRD, a single phosphine signal in the ^{31}P NMR spectrum indicated that the Pt atoms are located at the centers of the icosahedrons (Figure S18). A similar core structure was observed for $Au_{12}Ag_7(PMe_2Ph)_{10}(NO_3)_9$ and $Au_{17}Ag_2(PMe_2Ph)_{10}(NO_3)_9$ by Onaka and co-workers.[21] However, in these clusters four nitrates coordinate to the two Ag atoms at the vertex sites with an orthogonal orientation; thus $M_2Au_{17}(depp)_{10}Cl_7$ (**2**) has an unprecedented higher symmetry in its total structure. In the case of **2a**, the averaged bond lengths of Au–Au, Pd–Au, and Pd–Pd are 2.899(48), 2.760(44), and 2.559(1) Å, respectively (Figure 2f). The Pd–Pd bond length is remarkably shorter than that of bulk Pd (2.75 Å),[32] which in turn leads to a smaller Pd–Au–Pd bond angle than the typical angle observed for icosahedral structures (54.27(15)° vs. 60°). In the case of **2b**, the Pt–Pt bond length is also remarkably short at 2.567(1) Å,[33] causing a smaller Pt–Au–Pt angle of 54.03(13)° (Figure 2g). These severe distortions of the icosahedron are ascribed to the potent fusion of two icosahedral MAu_{12} cores sharing Au_5 facets.

Mass spectrometry measurements were used to further determine the composition of the synthesized nanoclusters **2a** and **2b** (Figures 3a,b). The positive-mode ESI-MS data showed clear peaks assignable to the monocation of $[M−Cl]^+$ $([M_2Au_{17}(depp)_{10}Cl_6]^+)$, whose isotope patterns were in good accordance with the simulated patterns, clarifying that $M_2Au_{17}(depp)_{10}Cl_7$ in the solution state has the same formula as that in the solid state determined by SCXRD.
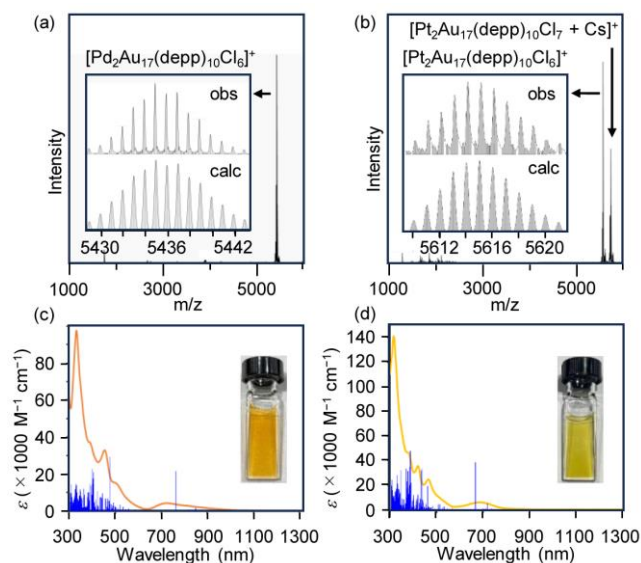

Figure 3. ESI-Mass spectra of (a) **2a** and (b) **2b**. Insets: observed and calculated isotope patterns of $[M−Cl]^+$. UV-vis absorption spectra of (c) **2a** and (d) **2b** in DCM. Blue lines are the TD-DFT-simulated optical spectra of (c) $Pd_2Au_{17}(PEt_3)_{10}Cl_7$ and (d) $Pt_2Au_{17}(PEt_3)_{10}Cl_7$.

Electronic absorption spectra were also measured to analyze the distribution of the MOs. The UV-Vis absorption spectrum of **2a** shows absorption bands at 730, 520, 490, and 360 nm (Figure 3c). Similar bands of **2b** were observed at 700, 460, and 420 nm, albeit with shifts to shorter wavelengths (Figure 3d). These newly observed absorption bands at longer wavelengths of 730 and 700 nm suggest the formation of new MOs around the frontier orbitals.
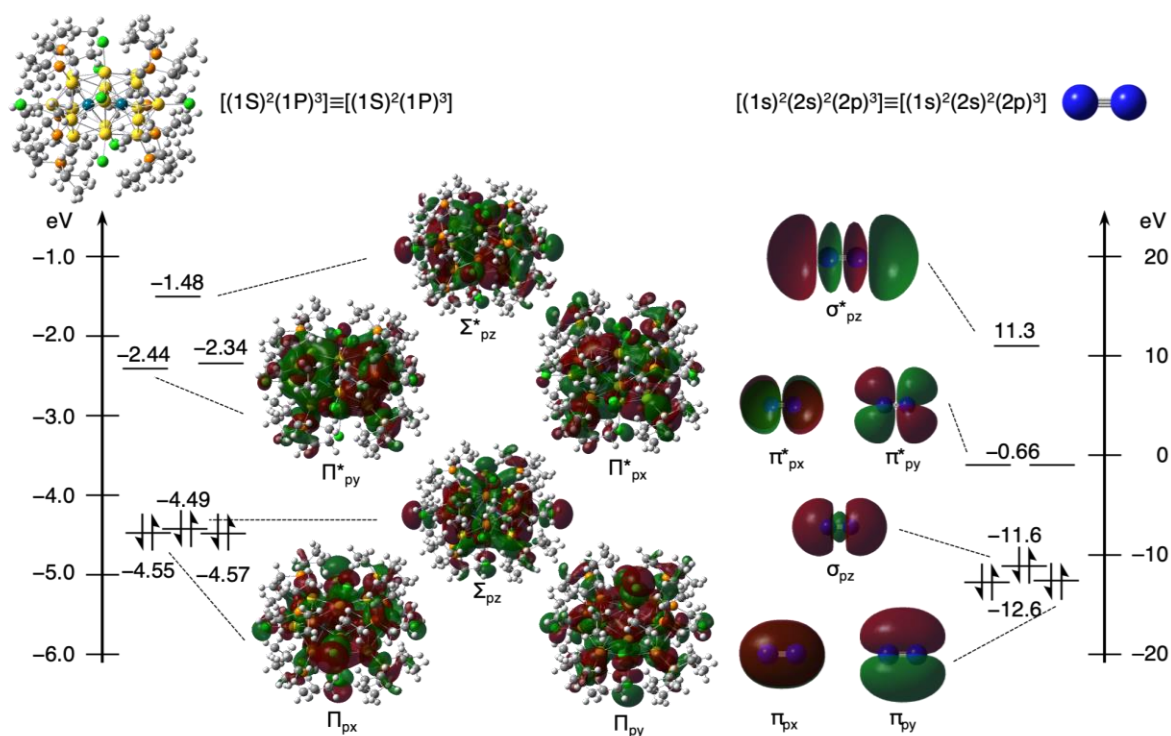

Figure 4. Energy diagrams and schematic Kohn–Sham orbitals of $Pd_2Au_{17}(PEt_3)_{10}Cl_7$ (left) and N_2 molecule (right).

DFT calculations showed the newly formed MOs using $Pd_2Au_{17}(PEt_3)_{10}Cl_7$ as the model system. The calculated MOs clearly indicate the formation of SAMOs between the two icosahedral MAu_{12} cores (Figure 4). HOMO, HOMO–1, and HOMO–2 are triply degenerate and can be viewed as Σ_{pz}, Π_{px}, and Π_{py} SAMOs formed by the linear combination of $1P_z$, $1P_x$, and $1P_y$ SAOs of each $PdAu_{12}$ core. Similarly, LUMO, LUMO+1, and LUMO+2 represent the Π^*_{py}, Π^*_{px}, and Σ^*_{pz} SAMOs, and HOMO–3 is Σ^*_s SAMO. The shape and order of energy levels of MOs of $Pd_2Au_{17}(PEt_3)_{10}Cl_7$ closely resemble those of N_2 molecule, indicating that nanoclusters 2 are N_2-type superatomic molecules having the electron configuration of $(1\Sigma)^2(1\Sigma^*)^2(1\Pi)^4(2\Sigma)^2$. To our best knowledge, they are the first experimentally and theoretically determined N_2-type superatomic molecules.

Further TDDFT calculations were performed to investigate the relationship between the electronic absorption properties and SAMOs. From the calculation results, the specific absorption of 2a at 730 nm is mainly attributed to the excitations from Π_{px} (HOMO–1) to Π^*_{px} (LUMO+1) and Π_{py} (HOMO–2) to Π^*_{py} (LUMO), which are transitions between SAMOs with the same symmetry (Figure 3c). Similarly, the excitation from Σ_{pz} (HOMO) to Σ^*_{pz} (LUMO+2) with the same symmetry contributes to the intense absorption at 490 nm. In contrast, the electron transition between SAMOs with different symmetry results in weaker excitations, for example $\Sigma_{pz} \rightarrow \Pi^*_{px}$, $\Sigma_{pz} \rightarrow \Pi^*_{py}$, $\Pi_{py} \rightarrow \Pi^*_{px}$, and $\Pi_{px} \rightarrow \Pi^*_{py}$ as the forbidden transitions. This electron excitation tendency, which depends on the symmetry of the SAMOs, strongly suggests that the SAMOs resemble conventional MOs in behavior. Similar absorption properties were observed for 2b (Figures 3d and S8). Previously, there have been only examples of F_2-type superatomic molecules whose Π^* SAMOs are fully occupied; there is no knowledge of electron transitions between Π and Π^* SAMOs.[9–12] This is the first report showing that the Laporte rule,[29] allowing electron excitations between MOs with the same symmetry, also applies to the electron excitation between SAMOs, similar to the MOs of conventional organic molecules.

Screening the reaction conditions can optimize the synthetic yields and provide insights into the reaction mechanism (Table 1).

Table 1. Screening of Reaction Conditions

$PdAu_{12}(depp)_8Cl_4$ **1a** $\xrightarrow[\text{solvent under Ar rt}]{\text{light additive (1 eq)}}$ $Pd_2Au_{17}(depp)_{10}Cl_7$ **2a**

entry	solvent (ratio)	time (h)	light (385-740 nm)	additive	yield (%)[b] 2a	RSM[d]
1	MeOH/DCM (3 : 1)	5	ON	–	59	–
2	MeCN/DCM (3 : 1)	5	ON	–	26	–
3	DCM	5	ON	–	23	58
4	MeOH/DCM (3 : 1)	24	OFF	–	–	quant
5	MeOH/DCM (3 : 1)	15	OFF	CAN[c]	25	–

[a]Reaction conditions: 1a (10.0 mg, 2.5 µmol), solvent (8 mL). [b]Yield was determined by the isolated yield per Pd or Pt. [c]CAN: ammonium hexanitraticerate(IV). [c]Recovered starting material 1a.

When visible light was irradiated onto the solution of 1a in a mixture of DCM and a polar solvent (MeOH and MeCN), an UV-Vis absorption spectral change occurred, and after 5 h of irradiation the cluster 2a was isolated in 59% and 26% yields (entries 1 and 2), respectively. On the other hand, when there was only a less polar solvent such as DCM, the spectral change was less after 5 h of reaction, resulting in 23% yield of 2a and recovery of the starting cluster 1a in 59% yield (entry 3). When the reaction was carried out in the dark, only negligible spectral changes were observed, and 1a was recovered completely irrespective of the solvent type (entry 4). These results indicate that the conversion from 1a to 2a requires both visible light and polar solvents. Conversely, when a conventional oxidation agent, ceric ammonium nitrate (CAN), was used, the cluster transformation reaction proceeded without visible light irradiation, affording cluster 2a in 25% yield (entry 5). This result strongly suggests that the photoinduced oxidation of cluster 1a is the key to this transformation.

The time-course ESI-MS measurements of 1a solution under exposure to indoor light (ca. 380–780 nm) provided information about the molecular weights of reaction intermediates (Figures 5). The freshly prepared solution of 1a in MeCN/DCM immediately generated many intermediates. Together with monocation species derived from the parent 8e cluster 1a, such as $[1a+Cs]^+$ and $[1a+Au(depp)]^+$, monocation species of one-electron oxidized 7e cluster $[PdAu_{12}(depp)_8Cl_4]^+$ 3a and two-electron oxidized/$[Au(depp)]^+$-detached 6e clusters $[PdAu_{11}(depp)_7Cl_4]^+$ 4a and $PdAu_{10}(depp)_6Cl_4$ 5a (observed as $[5a+Cs]^+$) were detected at 0 h (Figure 5a). After 3 h of irradiation by indoor light, 8e cluster 1a and 7e cluster 3a disappeared, and 6e clusters 4a and 5a were observed as the dominant species. After 24 h of reaction, the 10e cluster 2a was observed as the product together with 4a and 5a. These results suggest that the photoinduced oxidation and detachment of $[Au(depp)]^+$ are the key steps in this reaction, and 6e clusters 4a and 5a are the precursors for the dimerized product 2a. In contrast, the sample prepared in DCM solution retained the parent 8e cluster 1a as the major species, followed by 7e cluster 3a, and with minor contributions from 6e clusters 4a and 5a (Figure 5b). During the reaction, 3a became the major species, with the remaining 1a and generated product 2a. Even after 24 h of reaction, 1a and one-electron oxidized 7e cluster 3a were observed as the major species, suggesting that these two clusters are stable in DCM. This result agrees well with the fact that 59% of the starting cluster 1a was recovered from the reaction mixture in DCM (Table 1, entry 3). The high stability of 1a and 3a in DCM also indicates that the detachment of $[Au(depp)]^+$ is prohibited in DCM, suggesting that a polar solvent acts as a ligand to accelerate the detachment of $[Au(depp)]^+$ by coordinating to the vacant site. Li et al. recently reported a similar photoinduced detachment of $[Au(PR_3)]^+$ species from a phosphine/thiolate-co-protected $[Au_{25}(PR_3)_{10}(SR)_5Cl_2]^{2+}$ nanocluster in MeOH solution,[34] supporting that $[Au(depp)]^+$ is an intermediate in this reaction medium. The in-situ generated $[Au(PR_3)]^+$ species can act as an electron acceptor for photo-induced electron transfer from 1a, similar to the recently reported photoreducing property of the $PdAu_{12}$ cluster.[35] The formation of gold nanoparticles was confirmed during the reaction of 1a (Figure S9), which supports the proposed reduction of $[Au(PR_3)]^+$ species in the photoinduced process. Our proposed reaction mechanism for the photoinduced fusion of 1a is shown in Figure S10.
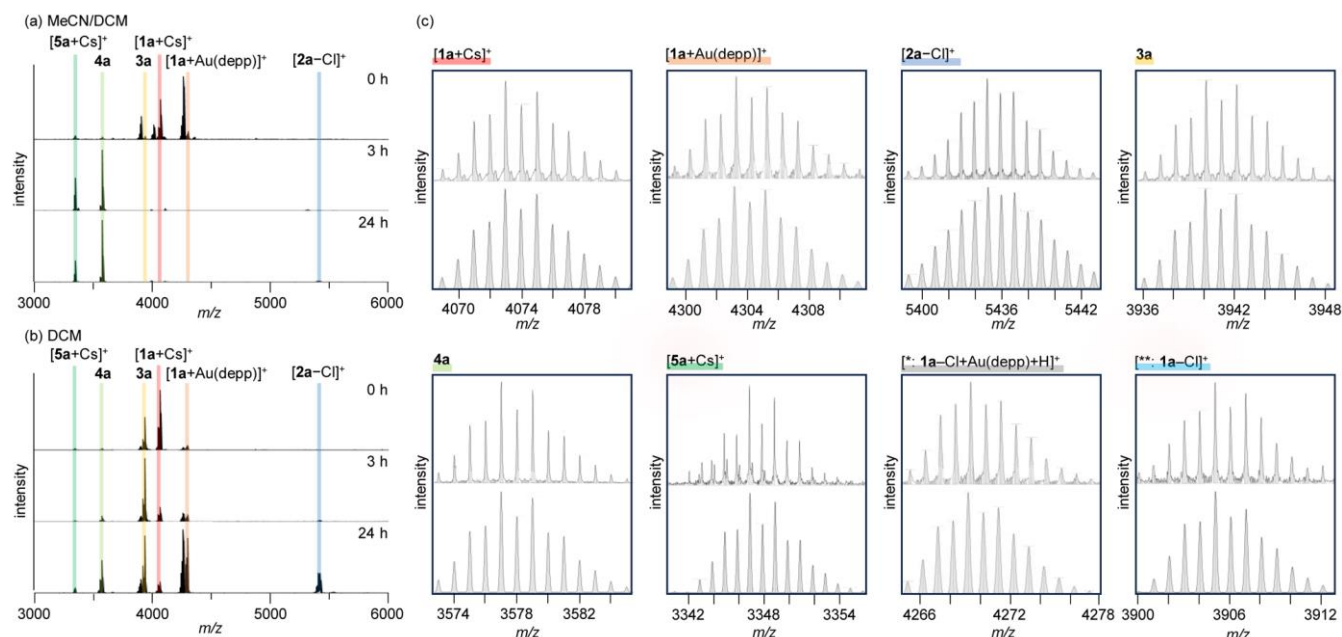
Figure 5. Time-course ESI-Mass spectra in the conversion of **1a** to **2a** under light irradiation: (a) MeCN/DCM and (b) DCM solutions. (c) Detected fragments (top) and theoretical isotopic patterns (bottom).

■ CONCLUSIONS

In summary, we discovered that the photoinduced fusion reaction of M@Au$_{12}$ superatoms affords novel M$_2$Au$_{17}$ nanoclusters featuring unprecedented N$_2$-like SAMOs. SCXRD analyses revealed the molecular structures of these clusters, in which the two fused M@Au$_{12}$ cores share Au$_5$ facets in the neutral form with 10 valence electrons. DFT calculations showed that the fused M@Au$_{12}$ superatoms form SAMOs by the linear combination of SAOs, resulting in an electron configuration of $(1\Sigma_s)^2(1\Sigma_s{}^*)^2(1\Pi_{px,\,py})^4(1\Sigma_{pz})^2$ comparable to that of N$_2$ molecule. TDDFT calculations demonstrated that the absorption properties of these superatomic molecules, like those of conventional molecules, depend on the symmetry of the SAMOs. Mechanistic investigations involving the screening of reaction conditions and time-course ESI-MS measurements showed that the fusion reaction of M@Au$_{12}$ superatoms is initiated by photoinduced oxidation and subsequent detachment of the [Au(PR$_3$)]$^+$ species. Although photoinduced structural transformation of gold and silver nanoclusters have been reported,[1,36–38] this is the first report on the inter-cluster fusion reaction. The photoinduced oxidation protocol will be useful to expand the library of metallic nanoclusters. This work not only demonstrates a new synthetic protocol for superatomic molecules but also enables a deeper understanding of the bonding theory of superatomic molecules.

ASSOCIATED CONTENT

Supporting Information

Detailed information about the instruments, materials, synthetic procedures, characterization, theoretical calculation, time-course UV-vis and ESI-Mass spectra from **1** to **2,** and plausible reaction mechanism.

Accession Codes

CCDC 2320633, 2320635, 2320641, 2321628 contain the supplementary crystallographic date for this paper. These data can be obtained free of charge via www.ccdc.cam.ac.uk/data_request/cif, or by emailing data_request@ccdc.cam.ac.uk, or by contacting The Cambridge Crystallographic Date Centre, 12 Union Road, Cambridge CB12, UK; fax: +44 1223 336033.

AUTHOR INFORMATION

Corresponding Author

Katsuhiro Isozaki – Institute for Chemical Research, Kyoto University, Kyoto 611-0011, Japan; Graduate School of Engineering, Kyoto University, Kyoto 615-8510, Japan; Email: kisozaki@scl.kyoto-u.ac.jp
Masaharu Nakamura - Institute for Chemical Research, Kyoto University, Kyoto 611-0011, Japan; Graduate School of Engineering, Kyoto University, Kyoto 615-8510, Japan; Email: masaharu@scl.kyoto-u.ac.jp

Author Contributions

RS found the formation of Pd$_2$Au$_{17}$ cluster and carried out all the experiments. KI carried out theoretical calculations. RS, MY, and KIS worked on the crystal growth, data collection, and structural analysis for X-ray single crystal analyses. KI and MN supervised the research and prepared the manuscript. All authors confirmed and finalized the manuscript and SI.

REFERENCES

(1) Zou, X.; Kang, X.; Zhu, M. Recent Developments in the Investigation of Driving Forces for Transforming Coinage Metal Nanoclusters. *Chem. Soc. Rev.* **2023**, *52*, 5892–5967.

(2) Li, Y.; Zhou, M.; Jin, R. Programmable Metal Nanoclusters with Atomic Precision. *Adv. Mater.* **2021**, *33*, 2006591.

(3) Kawawaki, T.; Ebina, A.; Hosokawa, Y.; Ozaki, S.; Suzuki, D.; Hossain, S.; Negishi, Y. Thiolate-Protected Metal Nanoclusters: Recent Development in Synthesis, Understanding of Reaction, and Application in Energy and Environmental Field. *Small* **2021**, *17*, 2005328.

(4) Omoda, T.; Takano, S.; Tsukuda, T. Toward Controlling the Electronic Structures of Chemically Modified Superatoms of Gold and Silver. *Small* **2021**, *17*, 2001439.

(5) Niihori, Y.; Miyajima, S.; Ikeda, A.; Kosaka, T.; Negishi, Y. Vertex-Shared Linear Superatomic Molecules: Stepping Stones to Novel Materials Composed of Noble Metal Clusters. *Small Sci.* **2023**, *3*, 2300024.

(6) Teo, B. K.; Zhang, H. Polyicosahedricity: Icosahedron to Icosahedron of Icosahedra Growth Pathway for Bimetallic (Au–Ag) and Trimetallic (Au–Ag–M; M = Pt, Pd, Ni) Supraclusters; Synthetic Strategies, Site Preference, and Stereochemical Principles. *Coord. Chem. Rev.* **1995**, *143*, 611–636.

(7) Cheng, L.; Yuan, Y.; Zhang, X.; Yang, J. Superatom Networks in Thiolate-Protected Gold Nanoparticles. *Angew. Chem. Int. Ed.* **2013**, *52*, 9035–9039.

(8) Cheng, L.; Yang, J. Communication: New Insight into Electronic Shells of Metal Clusters: Analogues of Simple Molecules. *J. Chem. Phys.* **2013**, *138*, 141101.

(9) Cheng, L.; Ren, C.; Zhang, X.; Yang, J. New Insight into the Electronic Shell of $Au_{38}(SR)_{24}$: A Superatomic Molecule. *Nanoscale* **2013**, *5*, 1475–1478.

(10) Qian, H.; Eckenhoff, W. T.; Zhu, Y.; Pintauer, T.; Jin, R. Total Structure Determination of Thiolate-Protected Au_{38} Nanoparticles. *J. Am. Chem. Soc.* **2010**, *132*, 8280–8281.

(11) Yuan, Y.; Cheng, L.; Yang, J. Electronic Stability of Phosphine-Protected Au_{20} Nanocluster: Superatomic Bonding. *J. Phys. Chem. C* **2013**, *117*, 13276–13282.

(12) Wan, X.-K.; Lin, Z.-W.; Wang, Q.-M. Au_{20} Nanocluster Protected by Hemilabile Phosphines. *J. Am. Chem. Soc.* **2012**, *134*, 14750–14752.

(13) Ito, E.; Ito, S.; Takano, S.; Nakamura, T.; Tsukuda, T. Supervalence Bonding in Bi-Icosahedral Cores of $[M_1Au_{37}(SC_2H_4Ph)_{24}]^-$ (M = Pd and Pt): Fusion-Mediated Synthesis and Anion Photoelectron Spectroscopy. *JACS Au* **2022**, *2*, 2627–2634.

(14) Ito, E.; Takano, S.; Nakamura, T.; Tsukuda, T. Controlled Dimerization and Bonding Scheme of Icosahedral $M@Au_{12}$ (M=Pd, Pt) Superatoms. *Angew. Chem. Int. Ed.* **2021**, *60*, 645–649.

(15) Kim, M.; Tang, Q.; Narendra Kumar, A. V.; Kwak, K.; Choi, W.; Jiang, D.; Lee, D. Dopant-Dependent Electronic Structures Observed for $M_2Au_{36}(SC_6H_{13})_{24}$ Clusters (M = Pt, Pd). *J. Phys. Chem. Lett.* **2018**, *9*, 982–989.

(16) Zhang, B.; Kaziz, S.; Li, H.; Wodka, D.; Malola, S.; Safonova, O.; Nachtegaal, M.; Mazet, C.; Dolamic, I.; Llorca, J.; Kalenius, E.; Lawson Daku, L. M.; Hakkinen, H.; Bürgi, T.; Barrabés, N. $Pd_2Au_{36}(SR)_{24}$ Cluster: Structure Studies. *Nanoscale* **2015**, *7*, 17012–17019.

(17) Negishi, Y.; Igarashi, K.; Munakata, K.; Ohgake, W.; Nobusada, K. Palladium Doping of Magic Gold Cluster $Au_{38}(SC_2H_4Ph)_{24}$: Formation of $Pd_2Au_{36}(SC_2H_4Ph)_{24}$ with Higher Stability than $Au_{38}(SC_2H_4Ph)_{24}$. *Chem. Commun.* **2012**, *48*, 660–662.

(18) Qian, H.; Barry, E.; Zhu, Y.; Jin, R. Doping 25-atom and 38-atom gold nanoclusters with palladium. *Acta Phys. Chim. Sin.* **2011**, *27*, 513–519.

(19) Liu, L.; Li, P.; Yuan, L.-F.; Cheng, L.; Yang, J. From Isosuperatoms to Isosupermolecules: New Concepts in Cluster Science. *Nanoscale* **2016**, *8*, 12787–12792.

(20) Yang, H.; Wang, Y.; Zheng, N. Stabilizing Subnanometer Ag(0) Nanoclusters by Thiolate and Diphosphine Ligands and Their Crystal Structures. *Nanoscale* **2013**, *5*, 2674–2677.

(21) Nunokawa, K.; Ito, M.; Sunahara, T.; Onaka, S.; Ozeki, T.; Chiba, H.; Funahashi, Y.; Masuda, H.; Yonezawa, T.; Nishihara, H.; Nakamoto, M.; Yamamoto, M. A New 19-Metal-Atom Cluster $[(Me_2PhP)_{10}Au_{12}Ag_7(NO_3)_9]$ with a Nearly Staggered–Staggered M_5 Ring Configuration. *Dalton Trans.* **2005**, 2726–2730.

(22) Zhu, M.; Eckenhoff, W. T.; Pintauer, T.; Jin, R. Conversion of Anionic $[Au_{25}(SCH_2CH_2Ph)_{18}]^-$ Cluster to Charge Neutral Cluster via Air Oxidation. *J. Phys. Chem. C* **2008**, *112*, 14221–14224.

(23) Zhu, M.; Aikens, C. M.; Hollander, F. J.; Schatz, G. C.; Jin, R. Correlating the Crystal Structure of A Thiol-Protected Au_{25} Cluster and Optical Properties. *J. Am. Chem. Soc.* **2008**, *130*, 5883–5885.

(24) Heaven, M. W.; Dass, A.; White, P. S.; Holt, K. M.; Murray, R. W. Crystal Structure of the Gold Nanoparticle $[N(C_8H_{17})_4][Au_{25}(SCH_2CH_2Ph)_{18}]$. *J. Am. Chem. Soc.* **2008**, *130*, 3754–3755.

(25) Dainese, T.; Antonello, S.; Bogialli, S.; Fei, W.; Venzo, A.; Maran, F. Gold Fusion: From $Au_{25}(SR)_{18}$ to $Au_{38}(SR)_{24}$, the Most Unexpected Transformation of a Very Stable Nanocluster. *ACS Nano* **2018**, *12*, 7057–7066.

(26) Takano, S.; Ito, S.; Tsukuda, T. Efficient and Selective Conversion of Phosphine-Protected $(MAu_8)^{2+}$ (M = Pd, Pt) Superatoms to Thiolate-Protected $(MAu_{12})^{6+}$ or Alkynyl-Protected $(MAu_{12})^{4+}$ Superatoms via Hydride Doping. *J. Am. Chem. Soc.* **2019**, *141*, 15994–16002.

(27) Takano, S.; Hirai, H.; Muramatsu, S.; Tsukuda, T. Hydride-Mediated Controlled Growth of a Bimetallic $(Pd@Au_8)^{2+}$ Superatom to a Hydride-Doped $(HPd@Au_{10})^{3+}$ Superatom. *J. Am. Chem. Soc.* **2018**, *140*, 12314–12317.

(28) Suyama, M.; Takano, S.; Nakamura, T.; Tsukuda, T. Stoichiometric Formation of Open-Shell $[PtAu_{24}(SC_2H_4Ph)_{18}]^-$ via Spontaneous Electron Proportionation between $[PtAu_{24}(SC_2H_4Ph)_{18}]^{2-}$ and $[PtAu_{24}(SC_2H_4Ph)_{18}]^0$. *J. Am. Chem. Soc.* **2019**, *141*, 14048–14051.

(29) Laporte, O.; Meggers, W. F. Some Rules of Spectral Structure. *J. Opt. Soc. Am.* **1925**, *11*, 459.

(30) Briant, C. E.; Theobald, B. R. C.; White, J. W.; Bell, L. K.; Mingos, M. P.; Welch, A. J. Synthesis and X-Ray Structural Characterization of the Centred Icosahedral Gold Cluster Compound $[Au_{13}(PMe_2Ph)_{10}Cl_2](PF_6)_3$; the Realization of a Theoretical Prediction. *J. Chem. Soc., Chem. Commun.* **1981**, 201–202.

(31) Lei, Z.; Li, J.; Nan, Z.; Jiang, Z.; Wang, Q. Cluster From Cluster: A Quantitative Approach to Magic Gold Nanoclusters $[Au_{25}(SR)_{18}]^-$. *Angew Chem Int Ed* **2021**, *60*, 14415–14419.

(32) Benfield, R. E.; Filipponi, A.; Bowron, D. T.; Newport, R. J.; Gurman, S. J.; Schmid, G. EXAFS Investigations of High-Nuclearity Pd Clusters. *Physica B: Condensed Matter* **1995**, *208–209*, 671–673.

(33) Feiten, F. E.; Takahashi, S.; Sekizawa, O.; Wakisaka, Y.; Sakata, T.; Todoroki, N.; Uruga, T.; Wadayama, T.; Iwasawa, Y.; Asakura, K. Model Building Analysis – a Novel Method for Statistical Evaluation of Pt L_3 -Edge EXAFS Data to Unravel the Structure of Pt-Alloy Nanoparticles for the Oxygen Reduction Reaction on Highly Oriented Pyrolytic Graphite. *Phys. Chem. Chem. Phys.* **2020**, *22*, 18815–18823.

(34) Zhang, J.; Wang, H.-D.; Zhang, Y.; Li, Z.; Yang, D.; Zhang, D. H.; Tsukuda, T.; Li, G. A Revealing Insight into Gold Cluster Photocatalysts: Visible versus (Vacuum) Ultraviolet Light. *J. Phys. Chem. Lett.* **2023**, *14*, 4179–4184.

(35) Hirai, H.; Takano, S.; Nakashima, T.; Iwasa, T.; Taketsugu, T.; Tsukuda, T. Doping-Mediated Energy-Level Engineering of $M@Au_{12}$ Superatoms (M=Pd, Pt, Rh, Ir) for Efficient Photoluminescence and Photocatalysis. *Angew. Chem. Int. Ed.* **2022**, *61*, e202207290.

(36) Qin, Z.; Wang, J.; Sharma, S.; Malola, S.; Wu, K.; Häkkinen, H.; Li, G. Photo-Induced Cluster-to-Cluster Transformation of $[Au_{37-x}Ag_x(PPh_3)_{13}Cl_{10}]^{3+}$ into $[Au_{25-y}Ag_y(PPh_3)_{10}Cl_8]^+$: Fragmentation of a Trimer of 8-Electron Superatoms by Light. *J. Phys. Chem. Lett.* **2021**, *12*, 10920–10926.

(37) Jana, A.; Jash, M.; Poonia, A. K.; Paramasivam, G.; Islam, M. R.; Chakraborty, P.; Antharjanam, S.; Machacek, J.; Ghosh, S.; Adarsh, K. N. V. D.; Base, T.; Pradeep, T. Light-Activated Intercluster Conversion of an Atomically Precise Silver Nanocluster. *ACS Nano* **2021**, *15*, 15781–15793.

(38) Tang, L.; Kang, X.; Wang, S.; Zhu, M. Light-Induced Size-Growth of Atomically Precise Nanoclusters. *Langmuir* **2019**, *35*, 12350–12355.

Ne-type superatom → N₂-type superatomic molecule
visible light
Ne   N≡N